





# Non-destructive electrochemical evaluation of corrosion protection systems subjected to accelerated ageing tests: a strategy for the conservation of colonial Mexican metal alloys

## Avaliação eletroquímica não destrutiva de sistemas de proteção contra corrosão submetidos a ensaios de envelhecimento acelerado: uma estratégia para a conservação de ligas metálicas do México colonial

**JAVIER REYES TRUJEQUE**<sup>1</sup>   
**LUIS ROMÁN DZIB PÉREZ**<sup>1\*</sup>   
**NORA ARIADNA PÉREZ CASTELLANOS**<sup>2</sup>   
**ARMANDO ARCINIEGA CORONA**<sup>3</sup> 

1. Laboratorio Nacional de Ciencias Para la Investigación y Conservación del Patrimonio Cultural-Centro de Investigación en Corrosión (LANCIC-CICORR), Universidad Autónoma de Campeche, Av. Agustín Melgar s/n, Col. Buenavista, C.P. 24039, San Francisco de Campeche, Cam., México

2. CONACYT-Instituto de Investigaciones Estéticas, Universidad Nacional Autónoma de México, Circuito Mario de la Cueva s/n, Ciudad Universitaria, Ciudad de México. C.P. 04510, México

3. Coordinación Nacional de Conservación del Patrimonio Cultural-Instituto Nacional de Antropología e Historia, Ex-convento de Churubusco S/N, San Diego Churubusco, Coyoacán, Ciudad de México, C.P. 04120, México

\*luidzib@uacam.mx

### Abstract

In this study we used Electrochemical Impedance Spectroscopy (EIS) to assess the protective capacity of different conservation treatments: benzotriazole, tannic acid and a polyurethane coating. They were applied on corroded coupons that replicate colonial Mexican brass and cast-iron alloys which were subjected to an accelerated ageing process under UVB/condensation exposure cycles. Electrochemical analysis was complemented with colorimetric measurements and FTIR analysis for information on the structural level before and after ageing. EIS results indicate that although the inhibitor systems prevent corrosion in early stages of the ageing, after 600 h they degrade, and corrosion products are formed resulting in low protective capacities. The selected polyurethane coating provided high protective capacities measured by EIS and agreed with no chemical degradation registered by FTIR and colour aspect. This investigation was performed with a methodology that can be replicated on site since it is non-destructive and the data can be employed for planning conservation strategies.

### Resumo

Neste estudo utilizamos a Espectroscopia de Impedância Eletroquímica (EIS) para avaliar a capacidade protetora de diferentes tratamentos de conservação, nomeadamente: benzotriazol, ácido tânico e revestimento de poliuretano. Os tratamentos foram aplicados em provetes corroídos que replicam latão colonial mexicano e ligas de ferro fundido submetidas a um processo de envelhecimento acelerado sob ciclos de exposição UVB/condensação. A análise eletroquímica foi complementada com medidas colorimétricas e FTIR para obter informações sobre o nível estrutural antes e após o envelhecimento. Os resultados do EIS indicam que, embora os sistemas inibidores previnam a corrosão nos estágios iniciais do envelhecimento, após 600 h os inibidores degradam-se e os produtos do processo de corrosão são formados, resultando numa baixa capacidade de proteção. O revestimento de poliuretano selecionado proporcionou grande capacidade de proteção (EIS), coincidente com os resultados obtidos por FTIR, por não apresentar degradação química ou mudanças na coloração. Esta investigação foi realizada com uma metodologia que pode ser replicada no local por ser não destrutiva, e os dados obtidos podem ser empregues para o planeamento de estratégias de conservação.

### KEYWORDS

Protective coatings  
 Brass  
 Cast iron  
 EIS  
 FTIR  
 SEM

### PALAVRAS-CHAVE

Revestimentos protetores  
 Latão  
 Ferro fundido  
 EIS  
 FTIR  
 SEM

## Introduction

For thousands of years, mankind explored materials from beneath the earth's surface and transformed them into spearheads, rudimentary tools and ornamental metal objects that have since corroded and can still be admired today. This legacy, left by our ancestors throughout history, are material goods that help us to define and understand cultural identities [1]. Hence, the interest in preserving this heritage in the best conditions and passing it on to future generations with the best guarantees of survival [2], even against the natural tendency of metals to corrode [3-4].

Historically, the conservation of metallic artefacts has followed rudimentary schemes that have evolved and become systematised over time. In recent decades, this has included both the maintenance of artefacts in controlled environments [5-6] and the use of oxide inhibitors, converters and anticorrosive coatings [7-12]. Benzotriazole (BTA) and tannic acid are the most widely used oxide inhibitors and converters, for copper [13-16] and iron alloys respectively [17-19]. BTA inhibitory action is explained by a physical barrier effect, which happens by the formation of a polymeric surface complex between the copper alloy corrosion products and BTA, due to the union of the triazole ring with the less noble metal of the alloy [13-14]. Several studies of BTA in aqueous solution showed that it induced a long-lasting prevention against corrosion, however, in outdoor environments, the protective capacity of BTA is lower [20-25]. In the case of tannic acid, it reacts with rust components, mainly iron oxides and oxyhydroxides, forming iron phosphates and tannates that induce the formation of surface layers with protective capabilities that prevent the corrosion progress [17]. However, the formation of these complexes provides a blue-black colour on the treated surfaces and their life period becomes short in outdoor environments [18-19]. In recent years, studies reported that the use of aliphatic polyurethane coatings provides strong dielectric layers that prevent current flow and combines good chemical and weather resistance with the possibility of selecting a matte, gloss, or colour finish accordingly. Therefore, polyurethanes are good candidates for applications on metallic heritage artifacts in order to obtain a better appearance and protection against corrosion but the efficiency is very dependent on the application method and coatings thickness [26-27].

On the other hand, to evaluate the behaviour of applied protection systems on metallic artifacts, it is very important the use of non-invasive and non-destructive techniques to avoid permanent damage on their physical, chemical and aesthetic properties. In this order, Electrochemical Impedance Spectroscopy (EIS) is an electrochemical technique that has been widely used in the evaluation of industrial paints and coatings. Recently, EIS has been implemented to study metallic heritage, because it has the advantage of applying a sinusoidal potential signal of 10-20 mV, small enough to avoid the alteration of the studied surface [28-33], and to measure the sinusoidal current response of the system with the same frequency, but of different amplitude and phase angle. In the same context, Fourier Transform Infrared Spectroscopy (FTIR), is an extremely useful spectroscopic technique for the interpretation of both organic and inorganic molecular structures. The infrared spectrum of a sample is obtained by recording the amount of energy absorbed at each wavelength of the incident infrared radiation [34-35, 36, pp. 137-196, 37]. This is achieved by scanning the spectrum with a monochromatic light that changes in wavelength over a time interval or by using a Fourier transform to measure all wavelengths at the same time. Thus, a spectrum of transmittance or absorbance can be traced, allowing the identification of bonds through the infrared energy absorbed by the sample [38-40].

In Mexico, metal heritage from the colonial period (seventeenth and eighteenth centuries) is abundant in outdoor environments such as cannonry and bells [41, pp. 37-39, 42]. These historic artefacts can be found in urban environments but the most degraded are on coastal cities subjected also to saline environments. In Mexico, conservators commonly employ corrosion inhibitors as the ones mentioned before, and the application of a polyurethane

coating commonly employed on industrial cases still needs to be evaluated for heritage artifacts.

Therefore, it was considered relevant to study the efficiency of different corrosion protection systems currently in use in Mexico by conservators with a specific reproducible methodology both in laboratory and directly on metal objects. This research evaluates the electrochemical behaviour of three protective systems on mockup coupons based on the colonial period alloys in Mexico: tannic acid for cast-iron, BTA for brass and a polyurethane coating was applied on both brass and cast-iron before and after an UV/condensation ageing period. In particular, the selected polyurethane coating is an industrial product that has the characteristic that can be applied directly to the metal without a primer or surface abrasion, no reversibility studies have been reported so far on this material.

## Experimental

### Preparation of the metal alloys coupons

In this study, representative cast-iron and brass coupons were manufactured considering the typical composition that these alloys had during the colonial period [43]. Table 1 shows the chemical composition (wt. %) of the 72 mockup coupons prepared (36 brass and 36 cast-iron) in comparison to the reported chemical compositions of brass and cast-iron during colonial period. For the experiment, coupons with dimensions of  $1.5 \times 2.0 \times 0.5$  cm for cast-iron, and  $2.0 \times 2.0 \times 0.5$  cm for brass were manufactured.

**Table 1.** Elemental composition obtained by SEM (wt. %) of brass and cast-iron coupons manufactured for this study, and typical composition of these alloys during the colonial period reported by Lopez-Garrido et al. [43].

Elemental content	Experimental brass coupons	Typical colonial brass alloy	Elemental content	Experimental cast iron coupons	Typical colonial cast-iron
Cu	67.8±0.4	72.3±0.5	Fe	90.1±0.6	85.0 ±0.6
Zn	22.0±0.2	20.3±0.3	C	4.3±0.8	5.6±0.2
C	5.4±0.3	3.1±0.1	Si	2.4±0.1	3.2±0.3
Sn	1.4±0.1	2.1±0.2	O	1.4±0.1	4.6±0.2
O	0.5±0.1	0.8±0.1	Mn	1.3±0.1	1.3±0.1

The coupons surface was progressively wet-ground to 1200 grit finish (SiC grit paper), washed with deionized water, and degreased using acetone. Then these coupons were oxidized. An artificial patina was grown on the brass samples by heating them up to 60 °C, then were immersed in a 2.0 wt. %  $K_2S$  solution, and after in a 1.0 wt. %  $CuSO_4$  solution and left to dry in a heating plate [44-45]. The cast-iron coupons were corroded by exposing them to an ISO type 3 natural marine atmosphere for three months to simulate alteration in a coastal city [46].

### Preparation of protective systems

The coupons were separated into two series, each series consists of 18 coupons for each alloy. The first series includes the inhibitor systems and the second series the polyurethane coating. The corroded coupons were prepared with the according protection system as presented in Table 2. For the first series of brass a 1 % of benzotriazole ethanolic solution was used (system 1). In the case of cast-iron, a 3 % tannic solution was prepared using ethanol, water and phosphoric acid to reach an acid pH (system 2) [47]. Both solutions were applied on the surface with a hand sprinkler.

The second series both brass and cast-iron coupons were treated with a commercial polyurethane coating Polylite 160-DTM prepared as the vendor indicated. An electrical low-pressure sprinkler was used for a homogeneous surface application (systems 3 and 4).

**Table 2.** Names and description of the applied protection system for each metal coupons.

Series	Base metal	Surface condition	Applied protection system	Name
1	Brass	Patinated	Benzotriazole (BTA)	System 1
	Cast-iron	Rusty	Tannic acid	System 2
2	Brass	Patinated	polyurethane coating	System 3
	Cast-iron	Rusty	polyurethane coating	System 4

### Accelerated ageing tests

All the systems were exposed to accelerated ageing tests in an ATLAS UV/CON chamber. The chamber operated in 4 × 4 h UVB/condensation exposure cycles according to the ASTM G-154-06 Standard [48] during a maximum time of 600 hours.

### Evaluation of the protection systems

For the materials characterization three coupons of each system before ageing (0 h) were considered control samples, then three coupons of each system were retired after 24, 96, 183, 384 and 600 hours of exposure for their analysis with the following techniques.

#### Fourier Transform Infrared spectroscopy (FTIR)

The FTIR analysis was carried out in an Alpha Reflectance Spectrophotometer (Bruker) in the middle infrared (500–4,000 cm<sup>-1</sup>) at 24 scans min<sup>-1</sup> and a spectral resolution of 4 cm<sup>-1</sup>. The data was processed with the Opus Video 7 software. For the data treatment, the OriginPro 8 software was used. Spectral identification was carried out by using the RRUFF electronic data bases and own FTIR spectra collection. The analysis was performed coinciding with the withdrawal periods of the samples.

#### Appearance and colorimetric measurements

The appearance of the samples was observed under optical microscopy in order to evaluate their appearance by using a stereomicroscope Stemi 305 (Carl Zeiss) coupled to an AxioCam 105 Camera (Carl Zeiss), after 24, 96, 183, 384 and 600 hours of ageing test.

Colour changes were measured by using a CM-700d spectrometer (Konica Minolta). It operated in the 400 to 700 nm visible range with a wavelength interval of 10 nm, spectral resolution of 0.01 % and an effective measure area of 3 mm. The data was analyzed by considering the CIE Lab colour system and the total colour change ( $\Delta E_{ab}^*$ ) before and after weathering was calculated by the following equation, defined by the Commission Internationale de L'Eclairage [49]:

$$\Delta E_{ab}^* = [(\Delta L^*)^2 + (\Delta a^*)^2 + (\Delta b^*)^2]^{1/2} \quad (\text{eq.1})$$

where:  $L^*$  indicates luminosity and variables  $a^*$  and  $b^*$  indicate the cartesian coordinates of the CIE Lab chromatic space.  $\Delta$  represents the difference between the trial and the reference value of the corresponding variable.

#### Electrochemical impedance spectroscopy (EIS)

Impedance measurements were carried out by using a Solartron Analytical 1280C Electrochemical Test System (Figure 1a), which was controlled by a personal computer using Z-plot software to operate the system and gather data. During EIS spectra acquisition, samples were potentiostatically held at their open circuit potential (OCP), a sinusoidal perturbation of 10 mV was applied to systems 1 and 2, and 20 mV to systems 3 and 4. The impedance response was measured in a frequency range from 20 KHz to 50 mHz.

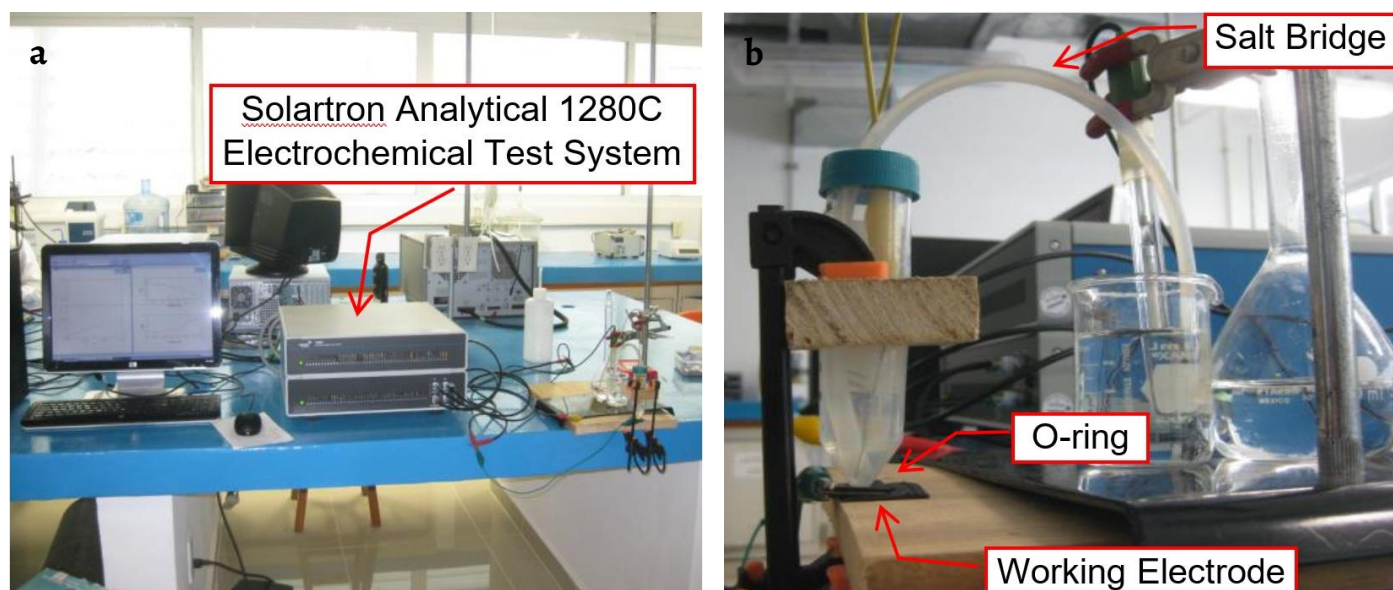


**Figure 1.** Experimental setup using: a) Solartron Analytical 1280C Electrochemical Test System and b) corrosion cell.

All electrochemical experiments were carried out in a neutral aerated 0.1 M  $\text{Na}_2\text{SO}_4$  solution, at  $25 \pm 1$  °C, using a three-electrode cell mounting (Figure 1b): the counter electrode was a platinum wire, an Ag/AgCl (KCl saturated) electrode was used as the reference electrode. The systems under study were the working electrodes. A rubber o-ring was used between the sample metallic and the cell to prevent solution leakage. The o-ring allowed a measurement area of 1 cm<sup>2</sup> to be exposed to the cell solution. To minimize the ohmic drop, the reference electrode was connected to the main cell compartment through of a salt bridge.

## Results and discussion

### Chemical and structural analysis

Figure 2 shows the FTIR spectra of the 1-2 and 3-4 systems, after 24, 96, 192, 384 and 600 h of accelerated ageing test. Control systems were included as well. Table 3 shows the corresponding FTIR absorption frequencies [50-56].

After 24, 96, 192, 384 and 600 hours of ageing, system 1 (Figure 2a and Table 3) showed a loss of the absorption signals corresponding to  $\nu_{\text{as}}(\text{N-N})$ ,  $\delta_{\text{oop}}(\text{C-C})$ ,  $\rho_{\text{as}}(\text{C-H})$  and  $\nu_{\text{as}}(\text{C-H})$  bonds, as well as a decrease in the intensity of the absorption bands associated to  $\sigma_{\text{as}}(\text{C-H})$  and  $\sigma_{\text{as}}(\text{N=N})$  bonds. These structural changes suggest a photochemical degradation of the polymeric complex that causes the loss of the protective capabilities in the complex due to mechanical, electrical, and optical transformations [17-19, 58].

Regarding system 2 (Figure 2b), the FTIR spectrum obtained after 24 h of ageing showed characteristic signals akin to those of the control system. However, a decrease in the intensity of the absorption band located in the range of 3200-3600 cm<sup>-1</sup> was also observed. This indicates the reduction of the free OH<sup>-</sup> groups, which allows the tannic acid to chelate the Fe ion [57, 59, pp. 144-160]. The FTIR spectra obtained after 96 and 192 h of ageing, showed a decrease in the intensity of the  $\nu_{\text{as}}(\text{C-O})$ ,  $\sigma_{\text{as}}(\text{C-H})$  and  $\sigma_{\text{as}}(\text{C-C})$  bonds while, the corresponding spectra for the 384 and 600 h of ageing showed the loss of the signal corresponding to the  $\nu_{\text{as}}(\text{C-O})$ ,  $\sigma_{\text{as}}(\text{C-C})$ ,  $\sigma_{\text{as}}(\text{C-H})$  and  $\delta_{\text{oop}}(\text{FePO}_4)$  bonds, this as consequence of the structural changes in the tannic acid molecule due to photodegradation [57, 59, pp. 144-160, 60-61].

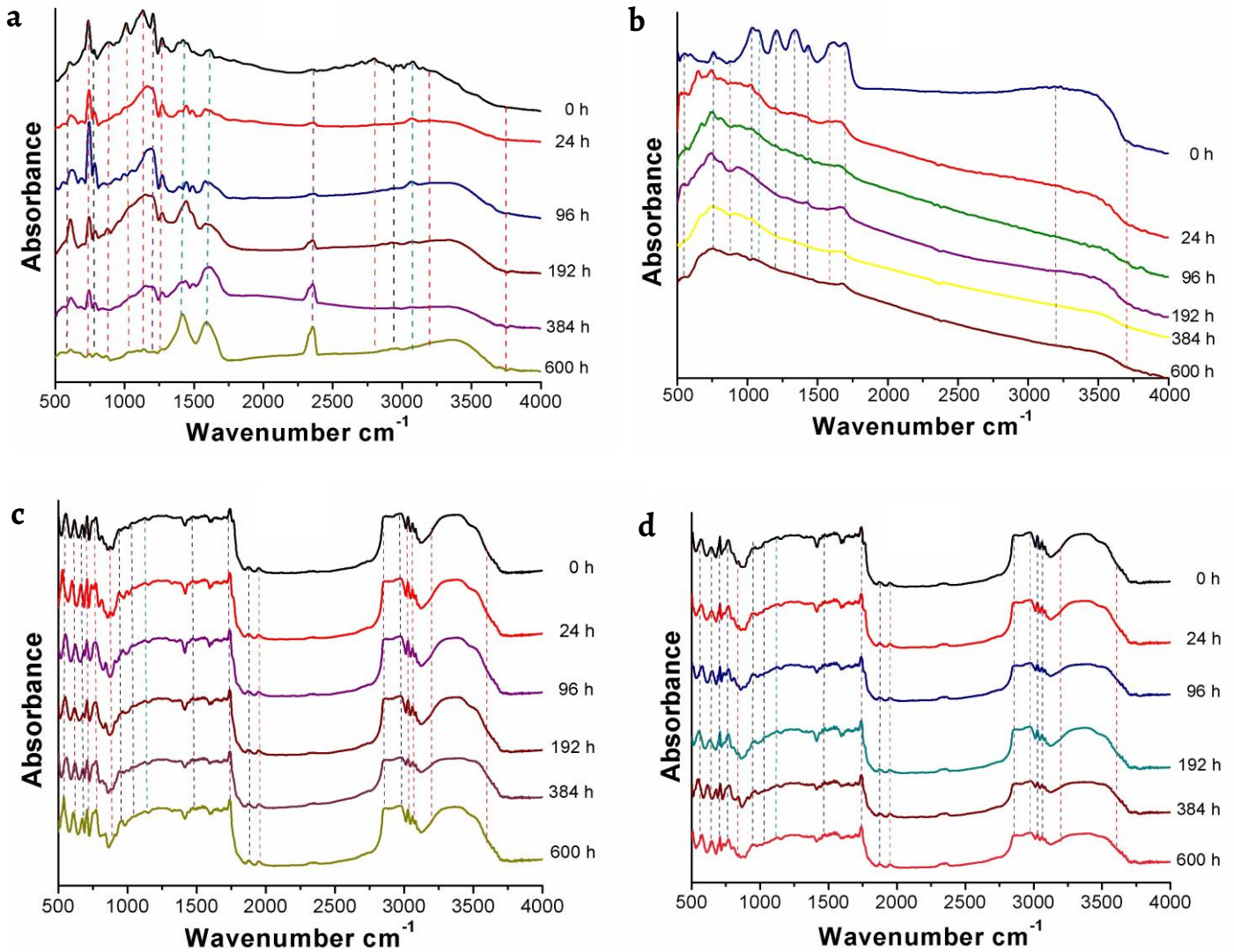


Figure 2. FTIR spectra of protective: a) system 1; b) system 2; c) system 3; d) system 4.

Figure 2c-d show the FTIR spectra after the ageing period of the systems 3 and 4 respectively. Not visible changes were observed in absorption intensities in comparison to the control system. This behaviour suggests that this coating conserves its structural stability after 600 h of ageing test, independently of the substrate where it was applied. This indicates that the polymer was not affected by exposure conditions. However, for longer exposure times, UV radiation could promote photo-oxidative degradation through a mechanism of free fall that starts when UV radiation is absorbed by the chromophore group causing the breakdown of the C-C bonds in the polymeric chain [62-67].

**Table 3.** FTIR absorption bands corresponding to the protective systems.

System 1				System 2			
Assigned signal	Band (cm <sup>-1</sup> )	Vibration mode	Reference	Assigned signal	Band (cm <sup>-1</sup> )	Vibration mode	Reference
Cu-O	606 (m)	$\nu_{as}$	[50]	Fe-O	550 (s)	$\nu_s$	[17]
C-H	740 (m)	$\sigma_s$	[51]	$\alpha$ Fe-O	760 (w)	$\nu_{as}$	
C-C	781 (w)	$\delta_{oop}$		$\alpha$ Fe-O	873 (w)	$\nu_{as}$	
N-N	871 (m)	$\nu_s$		$\gamma$ Fe-O	1035 (s)	$\nu_{as}$	
C-C	1007 (mw)	$\delta_{oop}$	[52-53]	$\gamma$ Fe-O	1080 (s)	$\nu_{as}$	
C-H	1127 (s)	$\sigma_s$		C-O	1207 (m)	$\nu_{as}$	[18-19]
N=N	1208 (m)	$\sigma_s$		C-H	1340 (w)	$\sigma_{as}$	
C-C	1246 (m)	$\nu_s$		C-C	1435 (m)	$\nu_s$	
C=C	1416 (m)	$\delta_{oop}$	[51]	FePO <sub>4</sub>	1620 (m)	$\delta_{oop}$	[57]
C=C	1617 (m)	$\delta_{oop}$		Fe (TH <sub>3</sub> ) <sup>l</sup>	1680 (m)	$\sigma_s$	
C-O	2353 (w)	$\nu_{as}$	[54]	O-H	3200-3600 (m)	$\nu_{s+as}$	[17]
C-H	2798 (m)	$\rho_{as}$	[51]				
C-H	2939 (w)	$\rho_{as}$					
C-H	3077 (s)	$\nu_s$					
O-H	3200-3600 (m)	$\nu_{s+as}$	[55-56]				

System 3				System 4			
Assigned signal	Band (cm <sup>-1</sup> )	Vibration mode	Reference	Assigned signal	Band (cm <sup>-1</sup> )	Vibration mode	Reference
C=C	555 (m)	$\delta_{iop}$	[59, pp. 144-160]	C-C	1473(m)	$\nu_s$	[60]
C=C	614 (m)	$\delta_{oop}$		C=C	1741 (m)	$\delta_{oop}$	[59, pp.144-160]
N-H	674 (w)	$\omega_{as}$		C=O	1877 (w)	$\nu_{as}$	[60-62]
C-H	701 (w)	$\delta_{iop+oop}$	[60-61]	C=O	1951 (w)	$\nu_{as}$	
C-H	779 (m)	$\delta_{iop+oop}$		CH <sub>2</sub>	2850 (w)	$\nu_{as}$	
C-H	875 (w)	$\sigma_s$	[60-62]	CH <sub>2</sub>	2971 (m)	$\nu_{as}$	
CH <sub>2</sub>	941 (w)	$\delta_{oop}$	[60]	CH <sub>2</sub>	3024 (w)	$\nu_s$	
C-H	1022 (s)	$\sigma_s$		C-H	3068 (m)	$\rho_s$	[60]
C-O	1120 (m)	$\nu_s$	[60-62]	O-H	3200-3600 (m)	$\nu_{s+as}$	[55]

\*s – strong; m – medium; mw – medium weak; w – weak; vw – very weak

### Appearance and colour evaluation

The appearance is an important aesthetic property to be considered in metallic artifacts corroded during its environmental interaction. Corrosion products aspect depends, of course, on the type of metal alloy, but also on the characteristic of the surrounding atmosphere (i.e. presence of sulphur dioxide, chloride, humidity, etc.), which also affects every preventive corrosion system applied over the artifact. Colour changes are one of the most important aspects to be evaluated in order to establish the long-term behaviour of metallic artifacts under corrosive environments.

During this study, the system appearance was monitored by optical microscopy and colour measurements. Figure 3 shows a set of surfaces microscopical images corresponding the four treatments during the control measurements at 24, 96, 192, 384 and 600 hours of ageing test.

System 1, had in appearance a homogeneous distribution of BTA, but during the first 192 h of exposure, occurred the formation of surface groves associated to the gradual loss of BTA. According to Roberge [68], those groves are preferential zones to initiate the corrosion process.

With the advance of ageing, the system turns cracked, with visible colour changes, consequence of the photochemical degradation of BTA [58, 68]. In the case of treatment 3, after 600 h of ageing, it does not present perceptible surfaces changes. It is indicative of the stability of the coating system under experimental conditions.

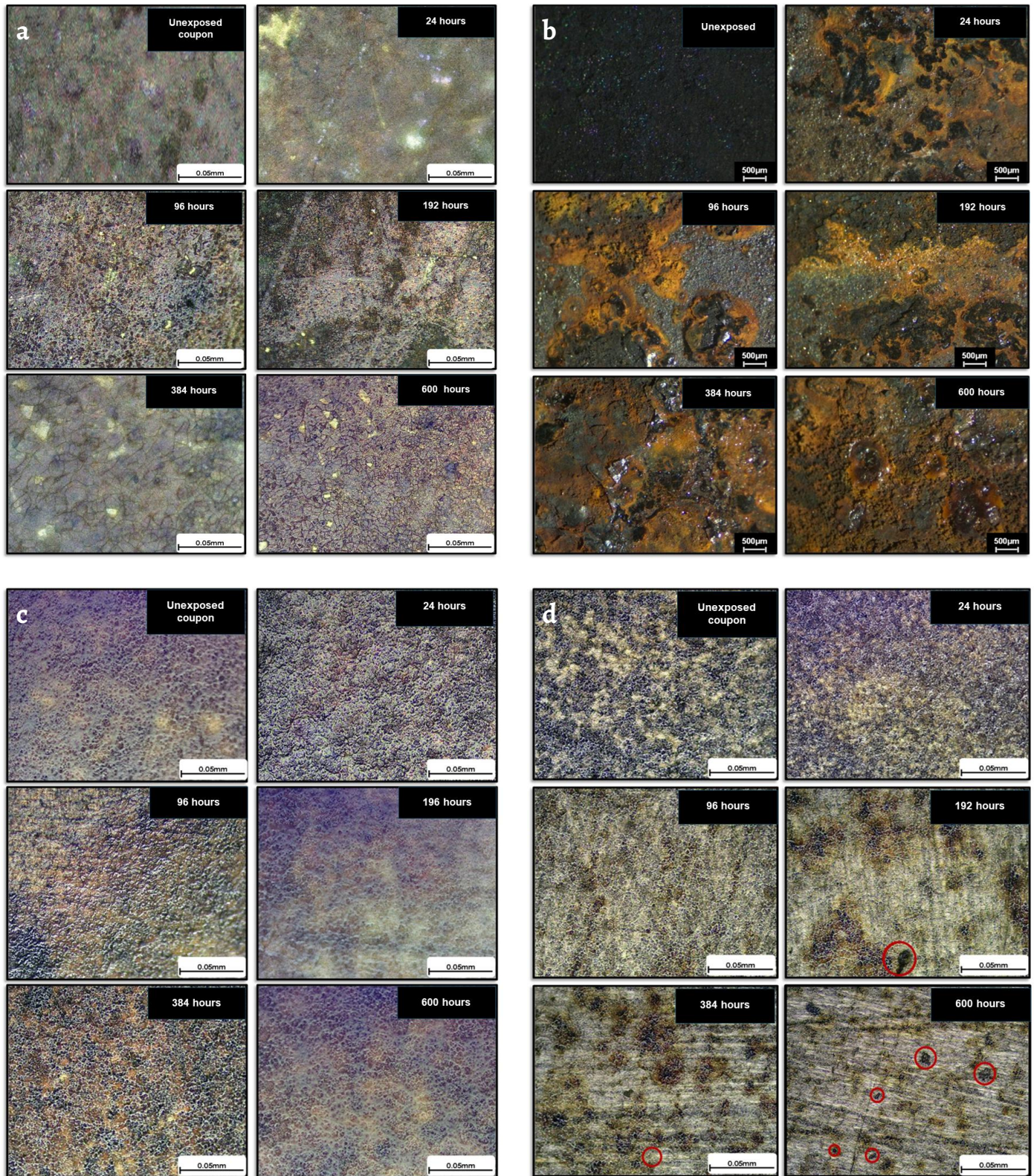


**Figure 3.** Evolution of the systems surface appearance registered by optical microscopy during the ageing test: *a)* system 1; *b)* system 2; *c)* system 3; *d)* system 4.

The images indicate that in apperency, the distribution of the coating systems applied over the iron coupon surface at the initiation of the experiment was homogeneous. After 24 h of ageing, the formation of blisters and the apparition of red to orange corrosion products result evident in system 3. After 96 h the formation and breakdown of blisters is frequent, resulting in the apparition of new corrosion products until the end of the experiment. It is known that the



breakdown of blisters is cause of the increase of corrosion rate, although, certain iron corrosion phase can be more stable when interact with the remnant tannic acid.

On the other hand, system 4 showed a more stable behaviour during the first 96 test hours, without apparent change in the coating appearance. Nevertheless, after 192 h of test, some picks, probable associated to the formation of pores in the de coating due to the photodegradation of the polymeric film start to appear [69]. They increase until the end of the experiment, and can be associated to the formation of localized zones where corrosion is possible.

The changes in the aesthetical aspect of the test systems were quantified through the colour measurements according to the CIELab system. Figure 4 show the colour evolution of the ageing coupons during the experiment, while Figure 5, indicates the tendency of the colour difference ( $\Delta E$ ) during the experiment.

The brass alloy used as muck-ups had an initial value of  $L^* = 71.2 \pm 2.9$ ,  $a^* = -7.1 \pm 0.9$  and  $b^* = 60.5 \pm 2.0$  corresponding to a brilliant yellow colour. After oxidation, these value change to  $L^* = 22.1 \pm 1.2$ ,  $a^* = -16.2 \pm 0.9$  and  $b^* = 28.4 \pm 2.0$  that corresponded to a dark brown colour. This colour changed when the system 1 was applied, diminishing its brightness and displacing to the red to- yellow zone. But when BTA was applied, the surface acquired whitish aspect. During ageing, surfaces changes induced by the continuous photodegradation of the inhibitor reach a  $\Delta E$  of 31 colour units (Figure 5). These visual changes could be an indicative of changes in stability of the coating, associated to the apparition of corrosion cells on brass surface [13, 15, 70-71].

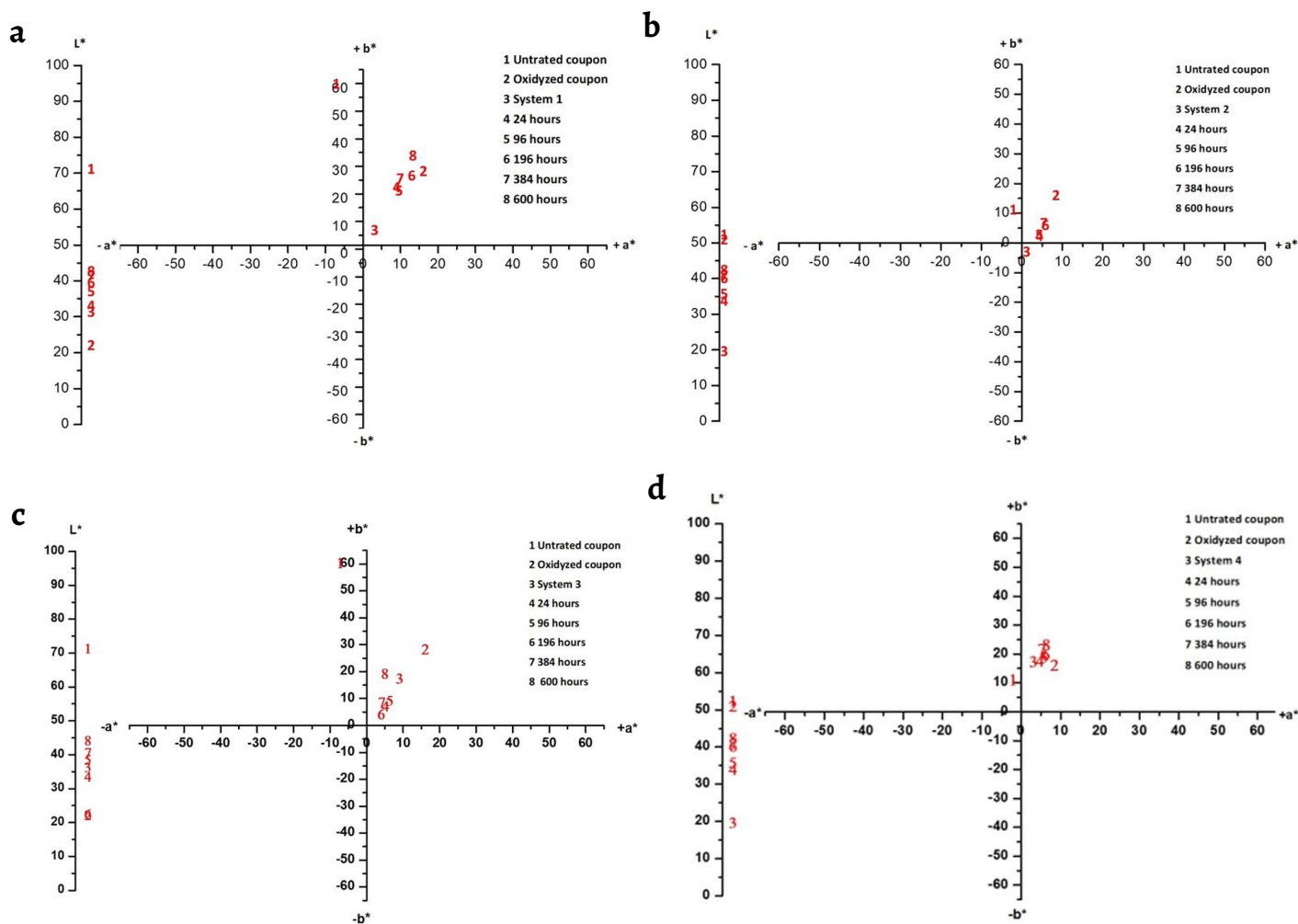
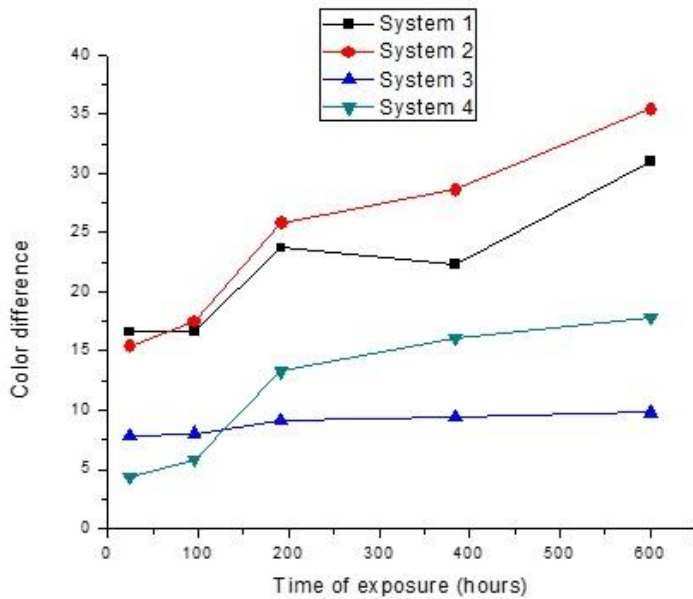


Figure 4. Colour coordinates for: a) system 1, b) system 2, c) system 3; d) system 4.



**Figure 5.** Evolution of colour change ( $\Delta E$ ) on the four test systems.

Cast iron muck ups showed initial  $L^* = 52.5 \pm 2.7$ ,  $a^* = -2.0 \pm 0.8$  and  $b^* = 11.2 \pm 1.1$  corresponding to a grey colour produced by graphite flakes present in the alloy [72]. After the oxidation, colour coordinates move to  $L^* = 51.1 \pm 1.7$ ,  $a^* = -8.4 \pm 0.3$  and  $b^* = 16.2 \pm 2.2$ , associated to the typical ochre colour of iron corrosion products (13). The application of tannic acid (system 3), scroll the colour to red to- blue with a lower luminosity, consequence of the formation of iron tannates. After ageing, the colour tends to the red to- yellow zone, with an increasing of luminosity. The system, reach a  $\Delta E$  of 35.4 when the experiment is over. Rendón [73], indicates that the colours orange and yellow are associated to the formation of the corrosion phases lepidocrocite and goethite respectively. Eventually, UV radiation photodegraded the chemical structure of tannates, then it caused the reactivation of corrosion process over metal surface [74].

By the other hand, the application of the polymer to systems 2 and 4 cause small variation in the visual aspect of the coupons, but it tends to change with the advance of the experiment. System 3 showed an initial  $L^* = 36.4 \pm 2.7$ ,  $a^* = 9.2 \pm 0.8$  and  $b^* = 17.5 \pm 0.01$  values, in the red to- yellow region. At the end of the experiment, the difference of colour was 9.8, closer to the perception limit for human eye [75]. For the system 4, the colour coordinates were  $L^* = 48.9 \pm 0.4$ ,  $a^* = 3.1 \pm 0.3$  and  $b^* = 17.5 \pm 0.7$ . At the end of the experiment,  $\Delta E$  was 17.9 colour units. In this order, colour changes started to be perceptible around 192 h after the experiment start up. Photodegradation of organic coating starts with the loss of the brilliance in the surface, followed by its disintegration. It affects the capabilities of the coating to protect the metallic surface again corrosion.

### Electrochemical analysis by EIS

Experimental impedance spectra of studies systems are presented in the form of Nyquist diagrams in Figure 6a, Figure 7a, Figure 8a and Figure 9a, as well as its respective Equivalent Circuit (EC). The impedance data were fitted using the Zview program.

#### System 1 (brass/patina/benzotriazole)

Figure 6a shows the Nyquist diagrams corresponding to system 1. There, two-time constants can be observed. The time constant at high frequencies is associated to the formation of the patina/BTA complex [16]. On the other hand, the time constant observed at low frequencies is attributed to the charge transfer caused by the corrosion process. It is associated to the presence of heterogeneities in the patina/BTA complex [14-15, 76]. The arc size of the time

constant at low frequencies decreases in accordance to the aging period. This suggests the loss of its protective capabilities in the polymeric complex as a result of the structural changes caused by the photodegradation [14-16, 76]. This behaviour was also consistent with the structural changes observed during the FTIR analysis.

The equivalent circuit showed in Figure 6a was used to interpret the EIS spectra of a one-layer oxide film structure. The parameter  $R_{sol}$  represents the electrolyte resistance used;  $CPE_{pbs}$  corresponds to the protective properties of the patina/BTA complex with a non-ideal model behaviour due to the presence of system irregularities, such as the lack of uniformity of the inhibitor, roughness, non-homogeneous distribution of the current, etc. [77-79]. On the other hand,  $R_{pbs}$  is the resistance associated to the patina/BTA complex.  $CPE_{dl}$  represents the electrochemical double-layer capacitance and  $R_{ct}$  is the charge transfer resistance that occurs at the metal-patina/BTA complex interface [13, 80-81]. This EC suggests the presence of defects in the complex, that according to Haruyama et al. [81], facilitates the interaction of the electrolyte with the metallic interface. Figure 6a shows the experimental data, in the form of symbols, and the fitted data, in the form of lines. The quality of the fit can be judged by observing the difference between the experimental and fitted values.

Figure 6b shows the decrease in the  $R_{pbs}$  y  $R_{ct}$  values as a function of ageing time, which suggests the loss of protective capabilities in the system. This behaviour is consequence of the photochemical degradation of the BTA, as suggested by Haruyama et. al., and Ling et. al. [13, 81], who assessed the electrochemical behaviour of BTA in copper specimens using polarization curves and EIS, respectively.

The capacitance of an electrochemical system is related to the quantity of material that can be transformed through the electrochemical processes [82-83]. In this study, the effective capacitance ( $C_{eff}$ ) associated to the CPE was calculated with equation 1, which is equivalent to that presented by Hsu and Mansfeld [84]:

$$C_{eff} = (Y_0 R_p^{1-n})^{1/n} \quad (1)$$

where  $n$ ,  $Y_0$  and  $R_p$  are the exponent, admittance constant of CPE and the parallel resistance associated to the faradaic process, respectively.

In Figure 6b, shows a progressive increase in the  $C_{pbs}$  y  $C_{dl}$  values, which suggests an increase in the corrosion rate. According to Fedrizzi et al. [83], the inhibitor photodegradation causes the appearance of defects that allow the continuous penetration of the electrolyte across the brass/patina interface, then an increase in corrosion rate occurs.

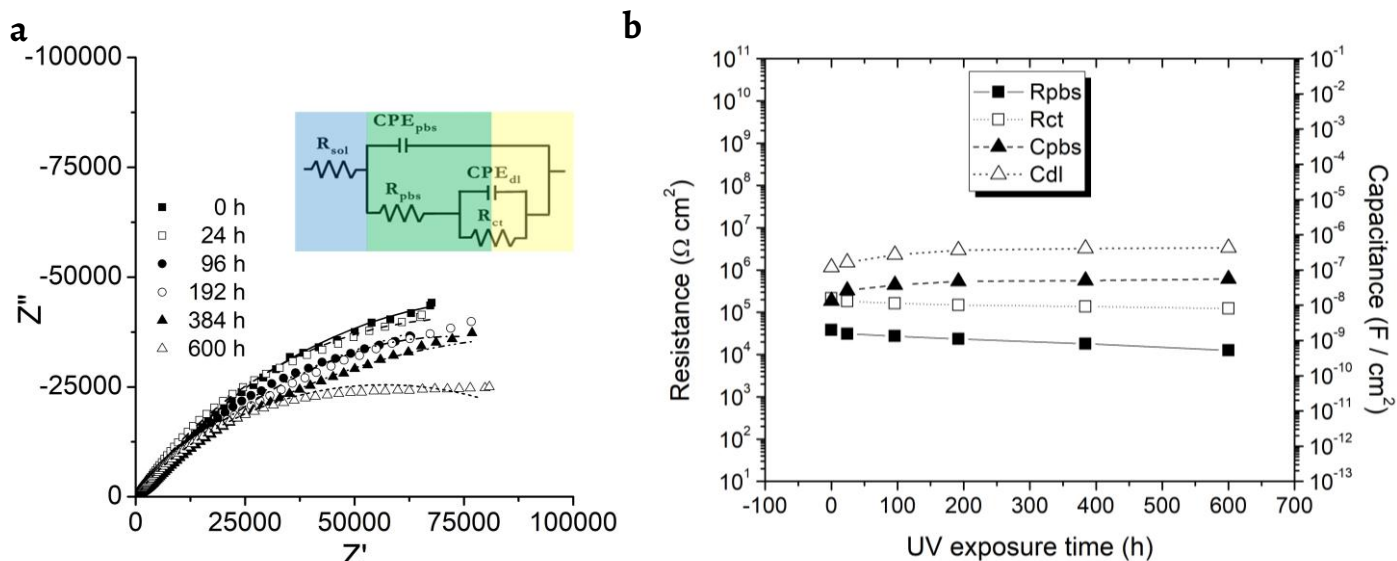


**Figure 6.** System 1: a) Nyquist plots and electrochemical circuit model used in fitting the experimental data, at different ageing times, exposed to 0.1 M  $Na_2SO_4$  solution; b)  $R_{pbs}$ ,  $R_{ct}$ ,  $C_{pbs}$  y  $C_{dl}$  values at different ageing time.

### System 2 (cast-iron/corrosion products/tannic acid)

During this study, all specimens of the system 2 presented one-time constant from high to intermediate frequencies (Figure 7a). That was associated to the formation of complexes formation between tannic acid and the substrate (phosphates and iron tannates) [18, 85].

At low frequencies, control specimens unexposed to ageing, tend to form a straight line with a slope of  $45^\circ$  (Figure 7a), which is typical of diffusion processes [18]. The experimental results obtained after 24 h of ageing showed the formation of a slope lower than  $45^\circ$ , with a tendency to form an arc. It can be associated to a change of diffusion to charge transfer processes caused by the metal/electrolyte interaction [85].

In the Nyquist diagrams, Figure 7a, can be observed that the impedance spectra start at different  $Z'$  values as function of ageing time; i.e., there is an increase in the electrolyte resistance. According to Orazem [86], this behaviour can be associated to the inhibitory effect produced by the substance that is deposited on the converted layer, which in contact with the electrolyte is solubilized, increasing the resistance of the medium due to the inhibitory ohmic effect of the active compound.

The arc size from the time constant at high frequencies increased as function of ageing time, probably due to the stability of the phases that were initially present as magnetite, goethite and lepidocrocite, which were observed during the FTIR characterization (Figure 2b). Those phases protect the base metal [87].

Figure 7a shows the EC model used to evaluate the impedance spectra for the unexposed system, where  $CPE_{co}$  and  $R_{co}$  are the capacitance and resistance associated with the layer of converted oxides, respectively [18, 50]. The use of Warburg impedance ( $Z_w$ ) suggests that the kinetics of the overall corrosion process of the studied system is controlled by the diffusion process, across the superficial porosities. Al-Mayouf [88], showed that the application of tannic acid on oxidized iron, allows the formation of a porous iron tannates layer, which is dependent on the moisture content. Figure 7a shows the EC model used to evaluate the impedance spectra when the system is under charge transfer control (for 24 – 600 hours exposure). These diagrams showed a good relation between experimental and fitted data using proposed models.

Figure 7b shows the increase in the  $R_{co}$  y  $R_{ct}$  values as function of ageing time, in contrast to the  $C_{co}$  and  $C_{dl}$  values which decreased. According to Favre [74], and Pantoja [89], these behaviours can be associated to the presence of a stable iron oxides phases of such as magnetite, goethite and lepidocrocite that provide good protective capabilities to the system.

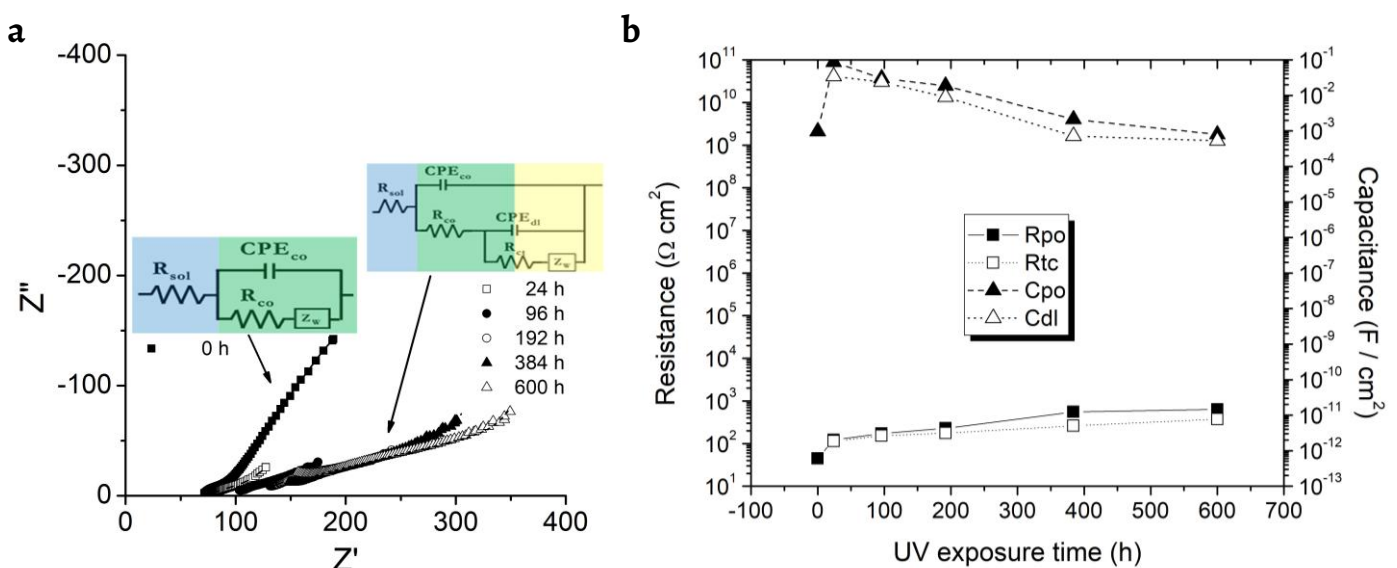


**Figure 7.** System 2: a) Nyquist plots and electrochemical circuit models used in fitting the experimental data, at different ageing times, exposed to 0.1 M  $\text{Na}_2\text{SO}_4$  solution; b)  $R_{co}$ ,  $R_{ct}$ ,  $C_{co}$  and  $C_{dl}$  values at different ageing time.

### System 3 (brass/patina/polyurethane coating)

The experimental results of EIS for system 3 (Figure 8a), shows a tendency toward the formation of a very big semicircle to high frequencies, from 20 KHz to 300 Hz. At lower frequencies scattered results were obtained, which are not presented in this study. This behaviour can be consequence of the formation of a homogeneous coating film which acts as an ideal capacitor that acts such as protective physical barrier of the metal surface, i.e., as an insulator, therefore, no charge transfer occurs [90-91]. Also, this behaviour is attributed to the lack of interactions between the electrolyte and the metal surface, hence the absence of a second or third time constant [92-93].

Figure 8a, presents the EC model used to evaluate the impedance spectra for system 3. The properties of the coating were evaluated by the pore resistance ( $R_{po}$ ) and a  $CPE_{po}$  that represents the capacitive properties of the protective layer formed by the polyurethane coating, as a consequence of its dielectric properties [94]. According to that, the protective mechanism of the polyurethane coating is barrier type, therefore, only one time constant was observed in the diagrams of Nyquist. The EC is similar to that used by Hu et al. [93], when organic coatings were evaluated at room temperature by using EIS.

Figure 8b shows the  $R_{po}$  and  $C_{po}$  values as a function ageing time.  $R_{po}$  values of coating decrease when the exposure time is increased. That suggests a reduction of the protective capacity of coating. However, the  $R_{po}$  are in the order of  $10^7 \Omega\text{-cm}^2$ , so according to Lee et. al. [95], this coating is in the range of medium protection. On the other hand,  $C_{po}$  values increased as a function ageing time. According to Martin et al. [92], it is possible that the degradation of coating allows the interaction of the metallic substrate with the electrolyte, causing the formation of preferential sites where corrosion can occur.

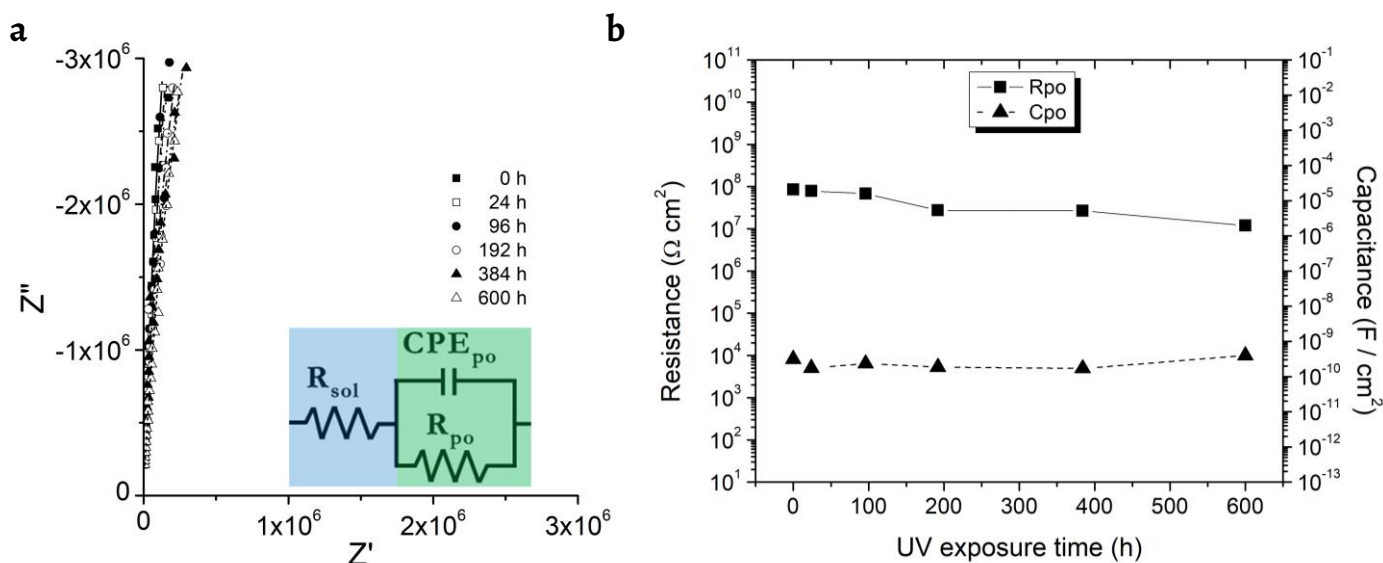


**Figure 8.** System 3: a) Nyquist plots and electrochemical circuit model used in fitting the experimental data, at different aging times, exposed to 0.1 M  $\text{Na}_2\text{SO}_4$  solution; b)  $R_{po}$  and  $C_{po}$  values for system 3 at different ageing time.

### System 4 (cast-iron/corrosion products/polyurethane coating)

In the Nyquist diagrams corresponding to system 4 (Figure 9a), two different behaviours can be observed. At high frequencies, the unexposed specimens and those with 24 and 96 h of ageing, shown a tendency to form a very large capacitive arc, similar to the observed in system 3 (Figure 8a), but as occurred with the system 3, the scattered results are not presented. The behaviour described, can be associated to the formation of a physical barrier that provides high values of dielectric resistance, directly related to good protection, as was previously observed in the Brass/Patina/POL system.

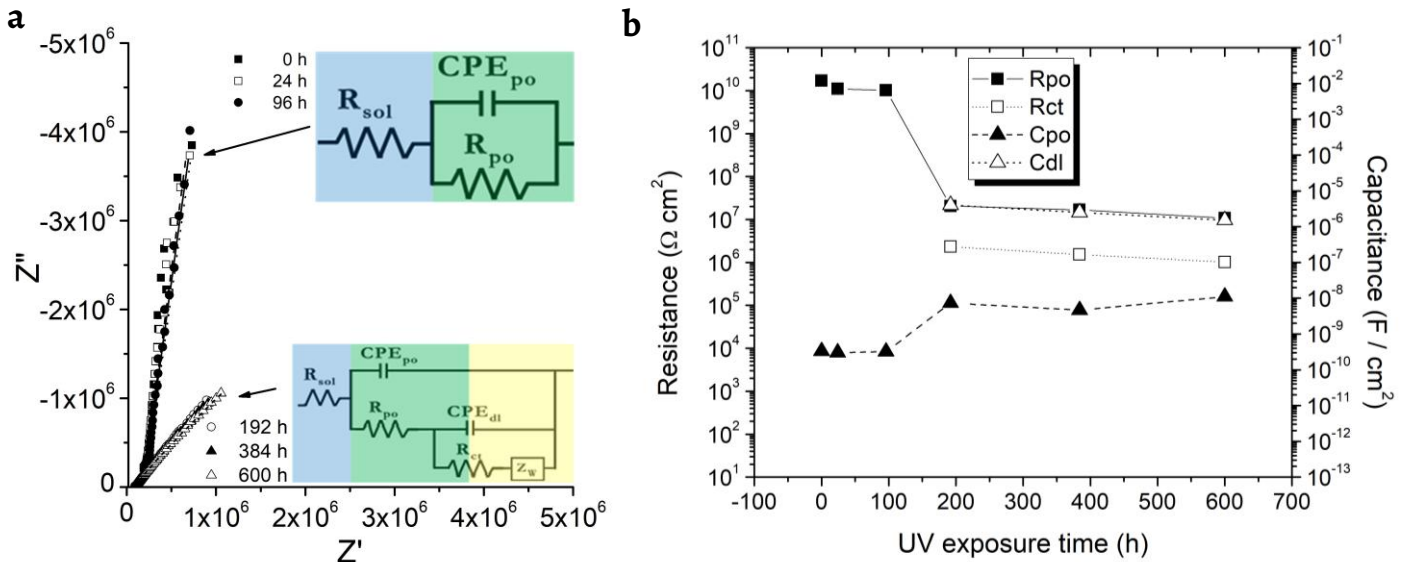


**Figure 9.** System 4: a) Nyquist plots and electrochemical circuit models used in fitting the experimental data, at different aging times, exposed to 0.1 M  $\text{Na}_2\text{SO}_4$  solution; b)  $R_{po}$ ,  $R_{ct}$ ,  $C_{po}$  and  $C_{dl}$  values for system 4 at different ageing time.

On the other hand, the experimental results obtained at 192, 384 and 600 h of ageing, shown a tendency to form an arc, of smaller size than that observed at initial times (Figure 9a). Vesga, indicates that this behaviour is associated to the appearance of coating defects such as pores, cracks or change of thickness, which allow apparition of diffusion process [96].

A Randles circuit [16] (Figure 9a) was used to analyze the impedance spectra for unexposed and exposed specimens after 24 and 96 h (very large capacitive arc). There  $R_{po}$  is the pore resistance and  $CPE_{po}$  represents the capacitive properties of polyurethane coating protective layer due to its dielectric properties [95-96].

To evaluate the impedance spectra that showed a decrease in the size of the arc (192, 384 and 600 h), associated with the coating failure, the circuit proposed by Haruyama et al. [81], was used (Figure 9a). Where  $CPE_{po}$ , at high frequencies, represents the dielectric properties of the coating that represent the non-ideal behaviours consequence of system irregularities such as lack of coating uniformity, roughness, non-homogeneous distributions of the current, etc.  $R_{po}$  is the resistance that provides the coating.  $CPE_{dl}$  is associated to the capacitance of the double layer,  $R_{ct}$  is the charge transfer resistance occurring in the metal-electrolyte interface [16] and  $Z_w$  is the Warburg impedance, used to adapt diffusional processes [96-97]. According to Itagaki et al. [77, 81], when a coating fails, corrosion occurred due to the combination of the following factors:

- diffusion of electrolyte ions toward the substrate through areas of the coating that present weak bonds;
- diffusion of the electrolyte by defects of the coatings such as air bubbles, craters, pores, etc. Then, the entry of oxygen induces the formation of anodic and cathodic sites in the substrate, in consequence corrosion reactions accelerate and a pH decrease occurs. This process can induce the loss of adhesion of the coating and metal surface.

Figure 9b shows the values of  $C_{po}$ ,  $R_{po}$ ,  $C_{dl}$  and  $R_{ct}$  as a function ageing time. At initial aging times, up to 96 h, the  $R_{po}$  values are in the order of  $10^9 \Omega \text{ cm}^2$ . From 192 h and until the end of aging, a decrease of 3 orders of magnitude was presented in the  $R_{po}$  values. Such a decrease can be associated to the appearance of defects in the coating, which allow the interaction of the electrolyte with the base metal resulting in the presence of a second arc in the Nyquist diagram, that corresponds to the corrosion process. The  $R_{ct}$  values also showed a tendency to decrease as the aging time increased as a result of the corrosion process. On the other hand, the  $C_{po}$  values

increased by around two magnitude orders from 192 h compared to those obtained at initial aging times. The  $C_{dl}$  values (associated to the  $R_{ct}$ ), increased when the exposure time increased.

According to Fedrizzi et al. [83], the increase in capacitance values ( $C_{po}$  y  $C_{dl}$ ) and the decrease in resistance values ( $R_{po}$  y  $R_{ct}$ ), are influenced by the appearance of defects in the coating that allow the formation of preferential sites where the corrosion process is carried out, suggesting an increase in the corrosion rate [83, 97-98].

## Conclusions

This study employed an electrochemical impedance spectroscopy analysis complemented with a set of surface instrumental analysis to assess protection systems on brass and cast-iron mockups from the colonial Mexican period. The results indicate that system 1 had a significant chemical degradation as showed by the FTIR analysis, the degradation of the surface after the ageing conditions can be observed by the naked eye since it had a high measured colour change, with  $R_{ct}$  values of approximately  $10^5 \Omega\text{-cm}^2$ . In system 2, the chemical degradation after ageing caused an observable colour change with a final  $R_{ct}$  values of  $376 \Omega\text{-cm}^2$ .

The systems protected with the polyurethane coating did not present chemical degradation and therefore the colour change was imperceptible to the naked eye though measured with the colorimeter. The physical barrier provided structural stability with  $R_{ct}$  values of the order of  $10^7 \Omega\text{-cm}^2$  for system 3. In system 4 the protective capacity was observed to decrease slightly with time due to thinning of the coating to a final  $R_{ct}$  value of the order of  $1 \times 10^6 \Omega\text{-cm}^2$ . Accordingly, the inhibitor protective systems could be recommended for indoors environment while the coating protective systems for outdoor.

These results showed that the non-destructive methodological proposal is adequate to gather information in a timeline basis on the corrosion processes that affect these cultural assets and can help the development of long-term preventive and corrective conservation strategies.

## Acknowledgements

This research was supported by the Project CONACYT LANCIC LN314886. The authors thanks to the CODICE Laboratory from CNCPC-INAH that supported with INAH project 11852, and the support of M. C. Emmanuel Chavez and to Dr. Jorge A. González Sánchez during the electrochemical test at CICORR-UAC. N.A.P. thanks to CONACYT Cathedra Program.

## REFERENCES

1. Watkinson, D., 'Preservation of metallic cultural heritage', in *Shreir's Corrosion*, 4th ed., vol. 4, ed. R. A. Cottis, Elsevier, London (2010) 3307-3340, <https://doi.org/10.1016/B978-044452787-5.00172-4>.
2. Llull-Peñalba, J., 'Evolución del concepto y de la significación social del patrimonio cultural', *Arte, Individuo y Sociedad* **17** (2005) 177-208.
3. Ávila Mendoza, J.; Genescá Llongueras, J., *Más Allá de la Herrumbre*, Fondo de Cultura Económica, México (1987).
4. Hihara, L. H., 'Electrochemical aspects of corrosion-control coatings', in *Intelligent Coatings for Corrosion Control*, ed. A. Tiwari, J. Rawlins and L.H. Hihara, Elsevier, London (2014) 1-15.
5. Angelini, E.; Grassini, S.; Mombello, D.; Neri, A.; Parvis, M.; Perrone, G., 'Plasma modified POF sensors for in situ environmental monitoring of museum indoor environments', *Applied Physics a Materials Science and Processing* **100**(3) (2010) 975-980, <https://doi.org/10.1007/s00339-010-5691-3>.
6. Corbellini, S.; Ferraris, F.; Neri, A.; Parvis, M.; Angelini, E.; Grassini, S., 'Exposure tolerant imaging solution for cultural heritage monitoring', *IEEE Transactions on Instrumentation and Measurement* **60**(5) (2011) 1691-1698, <https://doi.org/10.1109/TIM.2010.2090191>.
7. ICOM-CC, Terminology to characterize the conservation of tangible cultural heritage, New Delhi (2008), <http://www.icom-cc.org/54/document/terminology-to-characterize-the-conservation-of-tangible-cultural-heritage-english/?id=368> (accessed 2009-04-18).
8. Cano, E.; Lafuente, D.; Bastidas, D. M., 'Use of EIS for the evaluation of the protective properties of coatings for metallic cultural heritage: a review', *Journal of Solid State Electrochemistry* **14** (2010) 381-391, <https://doi.org/10.1007/s10008-009-0902-6>.
9. Fracassi, F.; d'Agostino, R.; Palumbo, F.; Angelini, E.; Grassini, S.; Rosalbino, F., 'Application of plasma deposited organosilicon thin films for the corrosion protection of metals', *Surface & Coatings Technology* **174-175** (2003) 107-111, [https://doi.org/10.1016/S0257-8972\(03\)00422-5](https://doi.org/10.1016/S0257-8972(03)00422-5).

10. Angelini, E.; Grassini, S., 'Plasma treatments for the cleaning and protection of metallic heritage artefacts', *Corrosion and Conservation of Cultural Heritage Metallic Artefacts* **25** (2013) 552–569, <https://doi.org/10.1533/9781782421573.5.552>.
11. Palumbo, F.; d'Agostino, R.; Fracassi, F.; Laera, S.; Milella, A.; Angelini, E.; Grassini, S., 'On low pressure plasma processing for metal protection', *Plasma Processes and Polymers* **6**(S1) (2009) 684–689, <https://doi.org/10.1002/ppap.200931704>.
12. Xu, W.; Han, E. H.; Wang, Z., 'Effect of tannic acid on corrosion behavior of carbon steel in NaCl solution', *Journal of Materials Science & Technology* **35**(1) (2019) 64–75, <https://doi.org/10.1016/j.jmst.2018.09.001>.
13. Ling Y., Guan Y, Han K. N., 'Corrosion inhibition of copper with benzotriazole and other organic surfactants', *Corrosion* **51**(5) (1995) 367–375, <https://doi.org/10.5006/1.3293601>.
14. Fateh, A.; Aliofkhaezrai, M.; Rezvani, A. R., 'Review of corrosive environments for copper and its corrosion inhibitors', *Arabian Journal of Chemistry* **13**(1) (2020) 481–544, <https://doi.org/10.1016/j.arabjc.2017.05.021>.
15. Lei, Y. H.; Sheng, N.; Hyono, A.; Ueda, M.; Ohtsuka, T., 'Effect of benzotriazole (BTA) addition on Polypyrrole film formation on copper and its corrosion protection', *Progress in Organic Coatings* **77**(2) (2014) 339–346, <https://doi.org/10.1016/j.porgcoat.2013.10.009>.
16. Gopi, D.; Govindaraju, K. M.; Collins, V.; Angelline, D. M.; Kavitha, L., 'A study on new benzotriazole derivatives as inhibitors on copper corrosion in ground water', *Corrosion Science* **51**(10) (2009) 2259–2265, <https://doi.org/10.1016/j.corsci.2009.06.008>.
17. Qian, B.; Hou, B.; Zheng, M., 'The inhibition effect of tannic acid on mild steel corrosion in seawater wet/dry cyclic conditions', *Corrosion Science* **72** (2013) 1–9, <https://doi.org/10.1016/j.corsci.2013.01.040>.
18. Barrero, C. A.; Ocampo, L. M.; Arroyave, C. E., 'Possible improvements in the action of some rust converters', *Corrosion Science* **43**(6) (2001) 1003–1018, [https://doi.org/10.1016/S0010-938X\(00\)00139-6](https://doi.org/10.1016/S0010-938X(00)00139-6).
19. Saji, V. S., 'Progress in rust converters', *Progress in Organic Coating* **127** (2019) 88–99, <https://doi.org/10.1016/j.porgcoat.2018.11.013>.
20. Cotton, J. B., 'The Control of Surface Reactions on Copper by means of Organic Compounds', in *Proceedings of the 2nd International Congress on Metallic Corrosion*, National Association of Corrosion Engineers, New York (1963) 590–596.
21. Cano, E.; Lafuente, D., 'Corrosion inhibitors for the preservation of metallic heritage artefacts', in *Corrosion and conservation of cultural heritage metallic artefacts*, European Federation of Corrosion series, eds. P. Dillmann, D. Watkinson, E. Angelini and A. Adriaens, WoodHead Publishing, Cambridge (2013) 570–594, <https://doi.org/10.1533/9781782421573.5.570>.
22. Dugdale, I.; Cotton, J. B., 'An electrochemical investigation on the prevention of staining of copper by benzotriazole', *Corrosion Science* **3**(2) (1963) 69–74, [https://doi.org/10.1016/S0010-938X\(63\)80001-3](https://doi.org/10.1016/S0010-938X(63)80001-3).
23. Finšgar, M.; Milošev, I., 'Inhibition of copper corrosion by 1,2,3-benzotriazole: a review', *Corrosion Science* **52**(9) (2010) 2737–2749, <https://doi.org/10.1016/j.corsci.2010.05.002>.
24. Cotton, J. B.; Scholes, I. R., 'Benzotriazole and related compounds as corrosion inhibitors for copper', *British Corrosion Journal* **2**(1) (1967) 1–5, <https://doi.org/10.1179/000705967798327235>.
25. Albini, M.; Letardi, P.; Mathys, L.; Brambilla, L.; Schröter, J.; Junier, P.; Joseph, E., 'Comparison of a bio-based corrosion inhibitor versus benzotriazole on corroded copper surfaces', *Corrosion Science* **143**(2018) 84–92, <https://doi.org/10.1016/j.corsci.2018.08.020>.
26. Bierwagen, G.; Tallman, D.; Li, J.; He, L.; Jeffcoate, C., 'EIS studies of coated metals in accelerated exposure', *Progress in Organic Coating* **46**(2) (2003) 149–158, [https://doi.org/10.1016/S0300-9440\(02\)00222-9](https://doi.org/10.1016/S0300-9440(02)00222-9).
27. Zhang, Y.; Maxted, J.; Barber, A.; Lowe, C.; Smith, R., 'The durability of clear polyurethane coil coatings studied by FTIR peak fitting', *Polymer Degradation and Stability* **98**(2) (2013) 527–534, <https://doi.org/10.1016/j.polymdegradstab.2012.12.003>.
28. Grundmeier, G.; Schmidt, W.; Stratmann, M., 'Corrosion protection by organic coatings: electrochemical mechanism and novel methods of investigation', *Electrochimica Acta* **45**(15–16) (2000) 2515–2533, [https://doi.org/10.1016/S0013-4686\(00\)00348-0](https://doi.org/10.1016/S0013-4686(00)00348-0).
29. Szocinski, M.; Darowicki, K., 'Local impedance spectra of organic coatings', *Polymer Degradation and Stability* **98**(1) (2013) 261–265, <https://doi.org/10.1016/j.polymdegradstab.2012.10.002>.
30. Zou, F.; Thierry, D., 'Localized electrochemical impedance spectroscopy for studying the degradation of organic coatings', *Electrochimica Acta* **42**(20–22) (1997) 3293–3301, [https://doi.org/10.1016/S0013-4686\(97\)00180-1](https://doi.org/10.1016/S0013-4686(97)00180-1).
31. Upadhyay, V.; Battocchi, D., 'Localized electrochemical characterization of organic coatings: a brief review', *Progress in Organic Coatings* **99** (2016) 365–377, <https://doi.org/10.1016/j.porgcoat.2016.06.012>.
32. Voulgaris, Ch.; Amanatides, E.; Mataras, D.; Grassini, S.; Angelini, E.; Rosalbino, F., 'RF power and SiO<sub>x</sub>CyHz deposition efficiency in TEOS/O<sub>2</sub> discharges for the corrosion protection of magnesium alloys', *Surface and Coatings Technology* **200** (2006) 6618–6622, <https://doi.org/10.1016/j.surfcoat.2005.11.058>.
33. Buchheit R. G., 'Corrosion resistant coatings and paints', in *Handbook of environmental degradation of materials*, 2nd ed., ed. M. Kutz, Elsevier, San Diego (2012) 539–568, <https://doi.org/10.1016/B978-081551500-5.50020-3>.
34. Bacci, M., 'UV-VIS-NIR, FT-IR, and FORS spectroscopies', in *Modern Analytical Methods in Art and Archaeology in Chemical Analysis*, eds. E. Ciliberto and G. Spoto, Wiley-interscience, New York (2000) 321–362.
35. Petit, S.; Madejova, J., 'Fourier Transform Infrared Spectroscopy', in *Handbook of Clay Science*, vol 5, eds. F. Bergaya and G. Lagaly, Elsevier, UK (2013) 213–231, <https://www.sciencedirect.com/bookseries/developments-in-clay-science/vol/5/suppl/C> (accessed 2024-05-09).
36. Pasto, D. J.; Johnson C. R., *Determinación de estructuras orgánicas*, Editorial Reverté, Barcelona (1981).
37. Dutta, A., 'Fourier Transform Infrared Spectroscopy', in *Spectroscopic methods for nanomaterials characterization*, vol 2, eds. S. Thomas, R. Thomas, A. K. Zachariah and R. K. Mishra, Elsevier, Amsterdam (2017) 73–93, <https://doi.org/10.1016/B978-0-323-46140-5.00004-2>.



38. Kumar, A.; Khandelwal, M.; Gupta, S. K.; Kumar, V.; Rani, R., 'Fourier Transform Infrared Spectroscopy: data interpretation and applications in structure elucidation and analysis of small molecules and nanostructures', in *Data processing handbook for complex biological data sources*, ed. G. Misra, Elsevier, London (2019) 77-96, <https://doi.org/10.1016/B978-0-12-816548-5.00006-X>.
39. Pickering, W. F., *Química analítica moderna*, Editorial Reverté, Barcelona (1980).
40. Bittner, R. W.; Hoffmann, H., 'Surface analysis: infrared spectroscopy', in *Reference Module in Chemistry, Molecular Sciences and Chemical Engineering*, 3rd edition, Elsevier Science, Oxford (2019) 1-15, <https://doi.org/10.1016/b978-0-12-409547-2.14385-9>.
41. Arano-Recio D., *Conservación de cañones de fundición de hierro del periodo colonial, que forman parte del patrimonio cultural de la ciudad de San Francisco de Campeche*, Master Dissertation, Department of Marine Science, Universidad Autónoma de Campeche, Campeche (2009).
42. Arano-Recio D., 'Proyecto "Restauración de vestigios de artillería": aspectos sobre la investigación y conservación de cañones con aleación de hierro de la ciudad de San Francisco de Campeche', *Revista Intervención* **4**(8) (2013) 47-53, <http://www.scielo.org.mx/pdf/inter/v4n8/v4n8a6.pdf> (accessed in 2024-05-09).
43. López Garrido, P. H.; González Sánchez, J. A.; Escobar Briones, E., 'Fouling communities and degradation of archeological metals in the coastal sea of the Southwestern Gulf of Mexico', *Biofouling* **31**(5) (2015) 405-416, <https://doi.org/10.1080/08927014.2015.1048433>.
44. Strandberg, H., 'Reactions of copper patina compounds - I. Influence of some air pollutants', *Atmospheric Environment* **32**(20) (1998) 3511-3520, [https://doi.org/10.1016/S1352-2310\(98\)00057-0](https://doi.org/10.1016/S1352-2310(98)00057-0).
45. Di Carlo, G.; Giuliani, C.; Riccucci, C.; Pascucci, M.; Messina, E.; Fierro, G.; Lavorgna, M.; Ingo, G. M., 'Artificial patina formation onto copper-based alloys: chloride and sulphate induced corrosion processes', *Applied Surface Science* **421**(A) (2017) 120-127, <https://doi.org/10.1016/j.apsusc.2017.01.080>.
46. ISO 9223:2012. 'Corrosion of metals and alloys - Corrosivity of atmospheres - classification, determination and estimation', International Organization for Standardization, ISO Central Secretariat, Geneva 20, Switzerland (2012).
47. Logan J., 'Tannic acid coating for rusted iron artifacts', in *Canadian Conservation Institute (CCI) Notes 9/5* (2014), <https://www.canada.ca/en/conservation-institute/services/conservation-preservation-publications/canadian-conservation-institute-notes/tannic-acid-rusted-iron-artifacts.html> (accessed in 2021-07-09).
48. ASTM G154-06, 'Standard practice for operating fluorescent light apparatus for UV exposure of nonmetallic materials', ASTM International, West Conshohocken, United States.
49. Marcus, R. T., 'The measurement of colour', in *Colour for science, art and technology*, ed. K. Nassau, Elsevier, Amsterdam (1997) 31-96.
50. Masi, G.; Esvan, J.; Josse, C.; Chiavari, C.; Bernardi, E.; Martini, C.; Bignozzi, M. C.; Gartner, N.; Kosec, T.; Robbiola, L., 'Characterization of typical patinas simulating bronze corrosion in outdoor conditions', *Materials Chemistry and Physics* **200** (2017) 308-321, <https://doi.org/10.1016/j.matchemphys.2017.07.091>.
51. Aziz, S. G.; Elroby, S. A.; Alyoubi, A.; Osman, O. I.; Hilal, R., 'Experimental and theoretical assignment of the vibrational spectra of triazoles and benzotriazoles. Identification of IR marker bands and electric response properties', *Journal of Molecular Modeling* **20**(3) (2014) 2078-2093, <https://doi.org/10.1007/s00894-014-2078-y>.
52. Shimanouchi, T., 'Tables of molecular vibrational frequencies', Consolidated Volume I, National Standard Reference Data System (NSRDS), NSRDS-NBS 39 (1972).
53. Mohamed, M. A.; Jaafar, J.; Ismail, A. F.; Othman, M. H. D.; Rahman M. A., 'Fourier Transform Infrared (FTIR) spectroscopy. Membrane characterization', in *Membrane Characterization*, eds. N. Hilal, A. F. Ismail, T. Matsuura and D. Oatley-Radcliffe, Elsevier, Amsterdam (2017) 3-29, <https://doi.org/10.1016/b978-0-444-63776-5.00001-2>.
54. Jinadasa, M. H.; Jens, K. J.; Øi, L. E.; Halstensen, M., 'Raman spectroscopy as an online monitoring tool for CO<sub>2</sub> capture process: demonstration using a laboratory rig', *Energy Procedia* **114** (2017) 1179-1194, <https://doi.org/10.1016/j.egypro.2017.03.1282>.
55. Bensebaa, F.; Ellis, T. H., 'Water at surfaces: what can we learn from vibrational spectroscopy?', *Progress in Surface Science* **50**(1-4) (1995) 173-185, [https://doi.org/10.1016/0079-6816\(95\)00052-6](https://doi.org/10.1016/0079-6816(95)00052-6).
56. Tranter, G. E., 'FTIR spectroscopy of aqueous solutions', in *Encyclopedia of spectroscopy and spectrometry*, vol 1, 3rd ed., eds. J. C. Lindon, G. E. Tranter and D. W. Koppenaal, Elsevier, Oxford (2017) 762-769, <https://doi.org/10.1016/B978-0-12-409547-2.12157-2>.
57. Hem, J. D., 'Complexes of ferrous iron with tannic acid', in *Chemistry of iron in natural water, Geological survey water-supply* **1459-D** (1960) 75-94, <https://doi.org/10.3133/wsp1459D>.
58. Borowska, E.; Felis, E.; Kalka, J., 'Oxidation of benzotriazole and benzothiazole in photochemical processes: kinetics and formation of transformation products', *Chemical Engineering Journal* **304** (2016) 852-863, <https://doi.org/10.1016/j.cej.2016.06.123>.
59. Félix de Castro, P., *Síntesis y caracterización de poliuretanos termoplásticos basados en policarbonato dioles. Relación estructura/propiedades*, PhD Dissertation, Department of Chemistry-Physic, Valencia University (2012), <http://hdl.handle.net/10550/25189>.
60. de Haseth, J. A.; Andrews, J. E.; McClusky, J. V.; Priester, R. D.; Harthcock, M. A.; Davis, B. L., 'Characterization of Polyurethane foams by mid-Infrared fiber/FT-IR spectrometry', *Applied Spectroscopy* **47**(2) (1993) 173-179, <https://www.osapublishing.org/as/abstract.cfm?URI=as-47-2-173>.
61. Reghunadhan, A.; Thomas, S., 'Polyurethanes: structure, properties, synthesis, characterization, and applications', in *Polyurethane polymers: blends and interpenetrating polymer networks*, eds. S. Thomas, J. Datta, J. T. Haponiuk and A. Reghundahan, Elsevier, Amsterdam (2017) 1-16, <https://doi.org/10.1016/B978-0-12-804039-3.00001-4>.
62. Rosu, D.; Rosu, L.; Cascaval, C. N., 'IR-change and yellowing of polyurethane as a result of UV irradiation', *Polymer Degradation Stability* **94**(4) (2009) 591-596, <https://doi.org/10.1016/j.polymdegradstab.2009.01.013>.
63. Cai, G.; Wang, H.; Jiang, D.; Dong, Z., 'Degradation of fluorinated polyurethane coating under UVA and salt spray. Part I: corrosion resistance and morphology', *Progress in Organic Coatings* **123** (2018) 337-349, <https://doi.org/10.1016/j.porgcoat.2018.07.025>.

64. Cai, G.; Zhang, D.; Jiang, D.; Dong, Z., 'Degradation of fluorinated polyurethane coating under UVA and salt spray. Part II: molecular structures and depth profile', *Progress in Organic Coatings* **124** (2018) 25-32, <https://doi.org/10.1016/j.porgcoat.2018.07.026>.
65. Hare, C. H., 'The degradation of coatings by ultraviolet light and electromagnetic radiation', *Journal of Protective Coatings & Linings* **May** (1992) LU-8029.
66. Wu, H., 'Highly accelerated UV weathering: when and how to use it', in *Service life prediction of polymers and plastics exposed to outdoor weathering*, eds. C. C. White, K. M. White and J. E. Pickett, Elsevier, Oxford (2018) 79-94, <https://doi.org/10.1016/B978-0-323-49776-3.00006-4>.
67. Schäfer, S. G.; Annamalai, V. E., 'Degradation of glass linings and coatings', *Reference Module in Materials Science and Materials Engineering* (2016) 1-11, <https://doi.org/10.1016/B978-0-12-803581-8.09241-9>.
68. Roberge, P. R., *Corrosion engineering – principles and practice*, McGraw Hills, New York (2008), <https://doi.org/10.1036/0071482431>.
69. Favaro, M.; Mendichi, R.; Ossola, F.; Russo, U.; Simon, S.; Tomasin, P.; Vigato, P. A., 'Evaluation of polymers for conservation treatments of outdoor exposed Stone monuments. Part I: photo-oxidative weathering', *Polymer Degradation and Stability* **91**(12) (2006) 3083-3096, <https://doi.org/10.1016/j.polyimdegradstab.2006.08.012>.
70. Sharma, V. C.; Shankar Lal U.; Singh, T., 'Method for stabilization of leaded bronzes affected by corrosion of lead', *Studies in Conservation* **48**(3) (2003) 203-209, <https://doi.org/10.1179/sic.2003.48.3.203>.
71. Díaz Martínez S.; García Alonso E., *Técnicas metodológicas aplicadas a la conservación-restauración del patrimonio metálico*, Ministerio de Cultura, España, (2010) 7-37.
72. Kumar, V.; Chaudhuri, S. K., 'Influence of alloying elements and microstructure on the corrosion behaviour of some low alloy steels', *Corrosion Reviews* **21**(4) (2003) 293-310, <https://doi.org/10.1515/CORRREV.2003.21.4.293/html>.
73. Rendón, J. L.; Valencia, A., 'Kinetics of structural rust transformation in environments containing chloride and SO<sub>2</sub>', *Revista de Metalurgia* **39**(extra) (2003) 9-14, <http://dx.doi.org/10.3989/revmetalm.2003.v39.iExtra.1089>.
74. Favre, M.; Landolt, D., 'The influence of gallic acid on the reduction of rust on painted steel surfaces', *Corrosion Science* **34**(9) (1993), 1481-1494, [https://doi.org/10.1016/0010-938X\(93\)90243-A](https://doi.org/10.1016/0010-938X(93)90243-A).
75. Keiman, A. C., *Propiedades ópticas de polímeros aplicado a pinturas decorativas*, Master Dissertation, Department Physical Sciences, Universidad Nacional Autónoma de México, México City (2011).
76. Saavedra-Torres, M.; Escobar, C. A.; Ocayo, F.; Tielens, F.; Santos, J., '1,2,3-Benzotriazole derivatives adsorption on Cu(111) surface: A DFT study', *Chemical Physics Letters* **689** (2017) 128-134, <https://doi.org/10.1016/j.cplett.2017.09.067>.
77. Itagaki, M.; Ono, A.; Watanabe, K.; Katayama, H.; Noda, K., 'Analysis on organic film degradation by dynamic impedance measurements', *Corrosion Science* **48**(11) (2006) 3802-3811, <https://doi.org/10.1016/j.corsci.2006.01.011>.
78. Touzain, S., 'Some comments on the use of the EIS phase angle to evaluate organic coating degradation', *Electrochimica Acta* **55**(21) (2010) 6190-6194, <https://doi.org/10.1016/j.electacta.2009.09.045>.
79. Pehkonen, S. O.; Yuan, S., 'Inorganic-organic hybrid coatings', *Interface Science and Technology* **23**(5) (2018) 115-132, <https://doi.org/10.1016/B978-0-12-813584-6.00005-3>.
80. Ramírez-Barat, B.; Cano-Díaz, E., 'Evaluación in situ de recubrimientos protectores para patrimonio cultural metálico mediante espectroscopía de impedancia electroquímica', *Grupo Español de Conservación* **8**(8) (2015) 6-13, <https://doi.org/10.37558/gec.v8i0.278>.
81. Haruyama, S.; Asari, M.; Tsuru, T., 'Corrosion protection by organic coatings', in *Electrochemical Society Proceedings*, eds. M. W. Kendig and H. Leidheiser, ECS, Pennington, 87 (2) (1987) 197-207.
82. Mendoza Flores, J.; Genescá Llongueras, J.; Durán Romero, R., *Espectroscopia de impedancia electroquímica en corrosión. Técnicas electroquímicas para el estudio de la Corrosión*, Academic notes, Universidad Nacional Autónoma de México, México City (2002) 53-91.
83. Fedrizzi, L.; Bergo, A.; Fanicchia, M., 'Evaluation of accelerated aging procedures of painted galvanized steels by EIS', *Electrochimica Acta* **51**(8-9) (2006) 1864-1872, <https://doi.org/10.1016/j.electacta.2005.02.146>.
84. Hsu, C. H.; Mansfeld, F., 'Technical note: Concerning the conversion of the constant phase element parameter Yo into a capacitance', *Corrosion* **57**(9) (2001) 747-748, <https://doi.org/10.5006/1.3280607>.
85. Popov, B. N., 'Basics of corrosion measurements', in *Corrosion engineering: principles and solved problems*, Elsevier, Amsterdam (2015) 181-237.
86. Orazem, M. E.; Tribollet, B., *Electrochemical impedance spectroscopy*, John Wiley & Sons, New Jersey (2009).
87. Zhao X. D.; Cheng, Y. F.; Fan, W.; Vladimir, C.; Volha, V.; Alla, T., 'Inhibitive performance of a rust converter on corrosion of mild steel', *Journal of Materials Engineering and Performance* **23**(11) (2014) 4102-4108, <https://doi.org/10.1007/s11665-014-1199-x>.
88. Al-Mayouf, A. M., 'Inhibitors for chemical cleaning of iron with tannic acid', *Desalination* **121**(2) (1999) 173-182, [https://doi.org/10.1016/S0011-9164\(99\)00018-1](https://doi.org/10.1016/S0011-9164(99)00018-1).
89. Pantoja-Castro, M. A.; González-Rodríguez, H., 'Study by infrared spectroscopy and thermogravimetric analysis of tannins and tannic acid', *Revista latinoamericana de química* **39**(3) (2011) 107-112.
90. MacDonald, J. R., 'Impedance spectroscopy', *Annals of Biomedical Engineering* **20** (1992) 289-305, <https://doi.org/10.1007/BF02368532>.
91. Halliday, D.; Resnick, R.; Krane, K. S., *Física Vol. 2*, 4th ed., Compañía Editorial Continental, México City (1999) 95-104.
92. Ángeles San Martín, M. E., *Efecto de la temperatura en la evaluación de recubrimientos anticorrosivos*, PhD Dissertation, Department of Chemistry, Universidad Nacional Autónoma de México, México City (2006).
93. Hu, J.; Li, X.; Gao, J.; Zhao, Q., 'UV aging characterization of epoxy varnish coated steel upon exposure to artificial weathering environment', *Materials and Design* **30**(5) (2009) 1542-1547, <https://doi.org/10.1016/j.matdes.2008.07.051>.

94. García-Ochoa, E.; Jayanthi, N.; Guadalupe Hernandez, J.; López-Montero, M.; Cruz, J.; Pandiyan, T., 'DFT and electrochemical studies: N,N',N'',N'''-tetrakis(2-methylpyridyl)-1,4,8,11-tetraazacyclotetradecane (TMPC) as an efficient corrosion inhibitor for carbon steel surfaces in an acid medium', *International Journal of Electrochemical Science* **8**(6) (2013) 8030-8049, [https://doi.org/10.1016/S1452-3981\(23\)12867-7](https://doi.org/10.1016/S1452-3981(23)12867-7).
95. Lee, C.; Mansfeld, F., 'Automatic classification of polymer coating quality using artificial neural networks', *Corrosion Science* **41**(3) (1999) 439-461, [https://doi.org/10.1016/S0010-938X\(98\)00127-9](https://doi.org/10.1016/S0010-938X(98)00127-9).
96. Vesga Lopez, L. F., *Estudio de los mecanismos de protección contra la corrosión de recubrimientos orgánicos usando espectroscopía de impedancia electroquímica (EIS)*, Master Dissertation, Escuela de Física, Universidad Industrial de Santander, Bucaramanga (2004).
97. Shreepathi, S.; Guin, A. K.; Naik, M. R.; Vattipalli, M. R., 'Service life prediction of organic coatings: electrochemical impedance spectroscopy vs actual service life', *Journal of Coatings Technology and Research* **8** (2010) 191-200, <https://doi.org/10.1007/s11998-010-9299-5>.
98. Miszczyk, A.; Darowicki, K., 'Multispectral impedance quality testing of oil – coating system using principal component analysis', *Progress in Organic Coatings* **69**(4) (2010) 330-334, <https://doi.org/10.1016/j.porgcoat.2010.07.003>.

RECEIVED: 2022.1.30

REVISED: 2022.6.1

ACCEPTED: 2024.5.20

ONLINE: 2024.6.20



This work is licensed under the Creative Commons Attribution-NonCommercial-NoDerivatives 4.0 International License. To view a copy of this license, visit <http://creativecommons.org/licenses/by-nc-nd/4.0/deed.en>.